JOURNAL OF MATERIALS SCIENCE 18 (1983) 353–364

Microanalytical investigation of sintered SiC

Part 1 *Bulk material and inclusions*

R. HAMMINGER, G. GRATHWOHL, F. THÜMMLER
Institut für Werkstoffkunde II, Universität Karlsruhe, Kernforschungszentrum Karlsruhe, Institut für Material- und Festkörperforschung, Postfach 3640, D-7500 Karlsruhe 1, West Germany

The microstructures and compositions of Al- and B-doped pressureless sintered SiC-materials from four different sources were investigated by the combined usage of several microanalytical techniques. Besides the fundamental ceramography and chemical analysis the methods of Auger electron spectroscopy (AES), wavelength dispersive analysis of X-rays (WDX), microautoradiography and scanning transmission electron microscopy (STEM) were used. In transgranular fractured surface regions the stoichiometric Si/C relation was found by AES. The grain boundaries, however, are enriched with C and O, and also partly with B and Al. Additives and impurities are distributed in an inhomogeneous manner; the heterogeneous inclusions are very differently sized from less than 0.1 μm (STEM) to 10 to 20 μm (WDX on polished specimens) and 200 μm (AES on fracture surfaces). These results reveal the need for improving the production process.

1. Introduction

The properties of non-oxide ceramics such as silicon carbide and silicon nitride are largely controlled by the presence and nature of second phases. In many production lines considerable amounts of additives are used in order to achieve products with a high density and a reasonable homogeneity. The densification behaviour is also influenced by the impurities of the starting powders. Additives and impurities can lead to a large scatter of the properties depending on their nature and their microstructural occurrence.

During recent years the pressureless sintering technique has been successfully developed for silicon carbide. This was possible by the use of small amounts of sintering additives. Since 1979 the originally used additives, i.e. B and C [1], can be replaced by other sintering aids such as Al and C [2]. For these Al-containing materials some technological advantages have been claimed [3] concerning the easier prevention of the exaggerated grain growth which eventually occurs at very high temperatures. Different suggestions are made in order to explain how these additives activate sintering, mainly with respect to de-oxidation effects and alternations of surface and grain-boundary energies [4], or to the occurrence of a liquid phase [5, 6], possibly with a transient nature. In spite of the fact that many properties of sintered silicon carbide are generally exciting, considerable scatter has been observed between materials from different sources. This is true for strength and for creep properties as well, measured in this laboratory [7].

The aim of this study was to characterize and analyse the microstructure of four different SSiC materials. The presence and microstructural parameters of second phases, inclusions, precipitations and the homogeneity of SiC grains have been investigated. The results are discussed with respect to their significance for the sintering and production process.

2. Experimental methods

Characteristic features of the microstructure of a high-quality sintered silicon carbide are the homogeneity, the very small grain size and minimized values of porosity and second-phase inclusions. Impurities and additives can be present in solid solution with silicon carbide, but also in the form of second phases. Because of their low concentration, microanalytical techniques with high resolutions are needed. Another problem exists in the nature of the sintering aids used: they are all

0022–2461/83/020353–12$03.94/0

TABLE I Methods and their specific objectives for the microanalytical investigation of SSiC

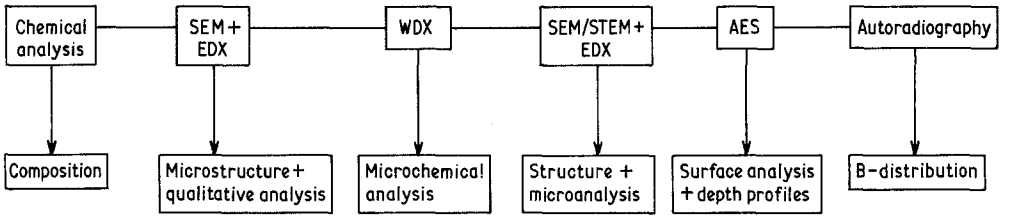

elements with very low atomic numbers, which generally cannot be analysed in a simple manner. To select suitable techniques the following points are of special importance:

(1) the atomic numbers of the elements which can be analysed qualitatively and/or quantitatively;
(2) the highest lateral resolution (depending on the working conditions and the specimen);
(3) information depth for given materials and working conditions;
(4) practicable detection limits;
(5) the possibility of depth analysis;
(6) the possibility of concentration profile analysis;
(7) statements about the chemical bonding;
(8) the coincidence of element signals;
(9) the error band of quantitative analyses.

In order to obtain comprehensive results, the combined usage of several techniques is necessary. The investigations of this study were performed by:

(1) chemical analysis;
(2) ceramography;
(3) scanning electron microscopy with energy dispersive analysis of X-rays (SEM/EDX);
(4) wavelength dispersive analysis of X-rays (WDX);
(5) transmission electron microscopy (TEM);
(6) scanning transmission electron microscopy with energy dispersive analysis of X-rays (STEM/EDX);
(7) Auger electron spectroscopy (AES);
(8) α-microautoradiography.

The specific objectives of these analytical methods are described in Table I.

3. Materials

Four pressureless sintered α-SiC materials were examined in this work. The materials I–IV were delivered in 1980 by four ceramic producers in Germany, USA and Japan. Different sintering additives were used as seen in Table II where the chemical analyses of the four materials are given. SSiC I represents an Al-doped material, while SSiC II, III and IV contain B as intentional sintering additive. The impurity content was very low at nearly the same level for all materials, while differences in the O and N content could be seen with a lower O content in materials II and IV, but with a higher N content in materials I and II.

All materials have high densities, as shown in Table III. The grain growth during sintering was controlled; exaggerated grain growth was not detected. Grain sizes no larger than 12 μm were found. The average grain size differed by a factor of less than 2 for the materials investigated; the values are given in Table III.

3.1. Ceramography and X-ray analysis

In all materials typical microstructural features such as large pores, cracks and inhomogeneities were found. They are possibly responsible for the moderate strength of the sintered SiC products, e.g. 400 to 500 MN m^{-2} [8]. In Fig. 1 some of these features, i.e. pores (a), orientated pores (b), inhomogeneities (c) and inclusions (d), are shown as observed by light microscopy on polished specimens.

TABLE II Chemical analyses of the SSiC materials investigated (n.d. = not determined)

Material	O	N	$C_{(free)}$	$Si_{(free)}$	Fe	Ca	Mg	Al	B	W	$C_{(tot)}$
SSiC I	0.10	0.07	< 0.51	< 0.20	< 0.1	< 0.05	< 0.01	0.40	< 0.1	< 0.1	29.5
SSiC II	< 0.01	0.055	< 0.50	< 0.50	< 0.05	< 0.05	< 0.1	0.05	0.34	< 0.1	30.4
SSiC III	0.08	0.03	< 0.54	< 0.2	< 0.1	< 0.05	< 0.01	< 0.1	0.25	< 0.1	30.9
SSiC IV	0.024	0.01	< 0.5	n.d.	0.065	< 0.02	< 0.01	0.015	0.225	n.d.	29.95

TABLE III Density and average grain size of the SSiC materials investigated

Material	Density (g cm^{-3})	Density (% theoretical density)	Average grain size (μm)
SSiC I	3.11	97.1	3.4
SSiC II	3.15	98.3	5.6
SSiC III	3.13	97.7	3.7
SSiC IV	3.10	96.4	4.0

After etching in boiling Murakami solution the microstructures of the specimens became visible. Scanning electron micrographs are shown in Fig. 2. It was found that the microstructure of the Al-doped material I differed from the B-doped materials mainly in two ways. First, the grains had a more uniform and smooth shape with a nearly elliptical form, while the B-doped materials exhibited more irregular and cleft grain forms. The other characteristic difference relates to the observation of parallel striation effects after etching, which were found only in the Al-containing material. These striation effects are usually considered to be caused by the $\beta \rightarrow \alpha$-phase transformation during sintering, but they may also be correlated with the preferred occurrence of the 2 H- and 4 H-polytypes. Using X-ray diffraction analysis it was determined that the Al-doped material consisted mainly of the 4 H-polytype, the B-doped SSiC of the 6 H-polytype. Thus, it can be assumed that the formation of the polytypes is influenced by the sintering additives. This is also confirmed by other experiments, where an increase in the 4 H-polytype was observed with increasing amounts of Al added [9]. In Fig. 2 it can also be seen that the surfaces of the grains do not lie in the same plane, especially for material I. This may point to a different method of attack of the etchant because of variable crystal orientations. Furthermore, the appearance of specimen III leads to the suggestion that some pores were generated during preparation, which may originally be filled with C or impurities. An SEM was used to study the fracture surfaces, shown in Fig. 3. Transgranu-

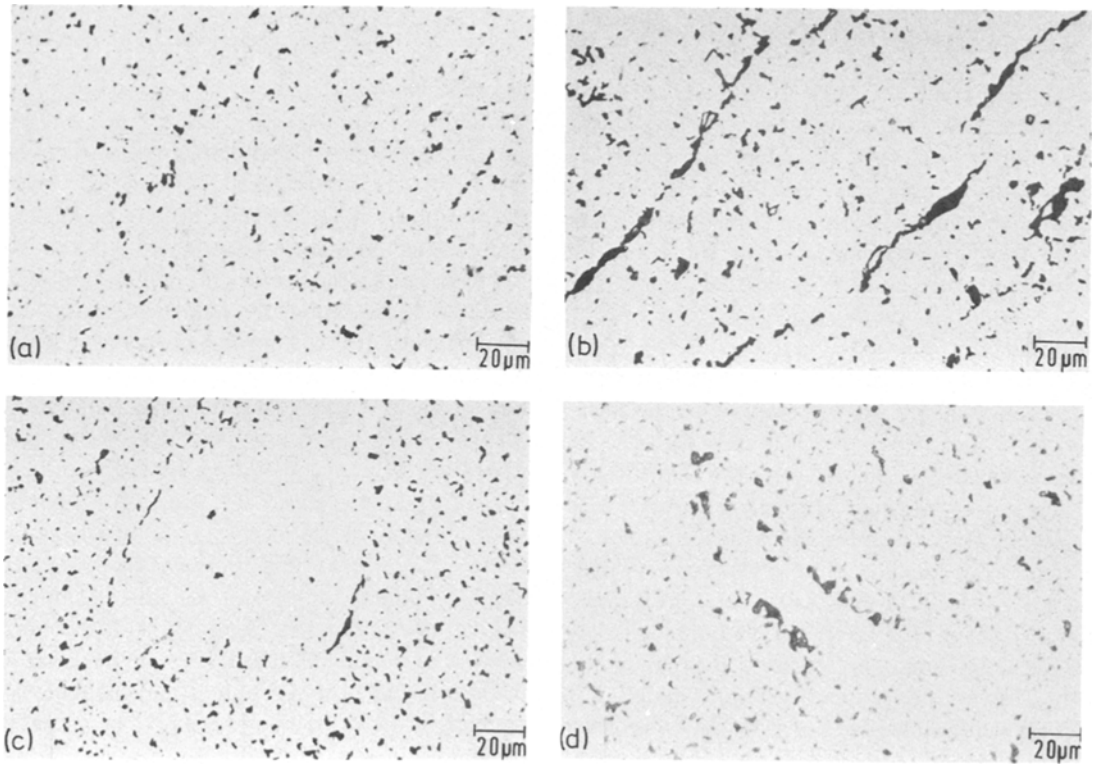

Figure 1 Optical micrographs of typical microstructural faults: (a) pores in SSiC I; (b) orientated pores in SSiC II; (c) inhomogeneities in SSiC III; (d) inclusions in SSiC IV.

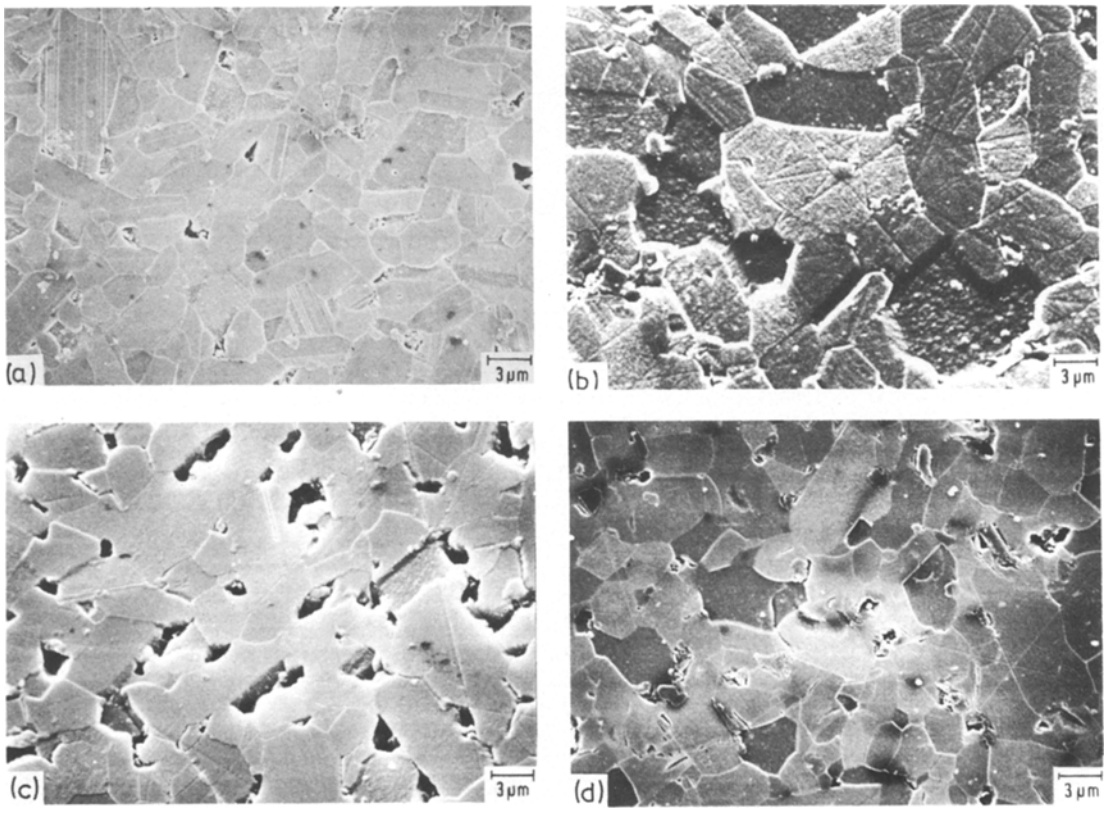

Figure 2 SEMs of etched specimens: (a) SSiC I; (b) SSiC II; (c) SSiC III; (d) SSiC IV.

lar and intergranular fracture modes were observed in all materials. The micrographs point to micropores and inclusions in all materials (see also Fig. 2). Some attempts were made, using SEM, to identify elements with atomic numbers larger than 11 by an energy dispersive system, but no quantitative results have been reached so far.

4. Results

4.1. Scanning Auger electron spectroscopy

Auger electron spectroscopy represents the chemistry of a few atom layers at the surface. The element analysis is generated by the identification of the energy of their characteristic Auger electrons. The Auger peak height is, in a first approximation, proportional to the element concentration. Fracture surfaces of materials I (Al-doped) and II (B-doped) have been investigated comprehensively. The measurements were performed in equipment with a lateral resolution of 2 to 3 μm. Working with acceleration voltages of 5 to 8 kV, the beam currents were about 0.2 to 3 μA. The specimens were fractured a short time before they were put into the working chamber; they were then cleaned in a smooth manner by the use of an argon ion beam.

The scanning electron micrographs of all investigated fracture surfaces (Fig. 3) show regions with trans- and intergranular fracture modes. In transgranular fractured surface regions the Si/C ratio was found as stoichiometric in principle. The microstructure of all specimens exhibit a large number of dark particles (Fig. 3), having an average diameter of 1 μm. These particles were identified as free carbon by the use of a high resolution AES equipment.

The Al-doped sample showed Al-rich areas of different sizes and with a heterogeneous distribution. These areas are generally connected with enrichments of C and O. A very large area ($2.0 \times 0.5\ mm^2$) of this type was investigated in depth by bombarding with argon ions ($12\ nm\ h^{-1}$). During sputtering, the high O- and C-contents were very rapidly reduced, the Si-concentration increased, while the Al-content remained virtually unchanged up to a depth of 1.4 μm where the investigation was stopped. The profiles are presented in Fig. 4. The final Si/C relation was lower than in pure SiC matrix.

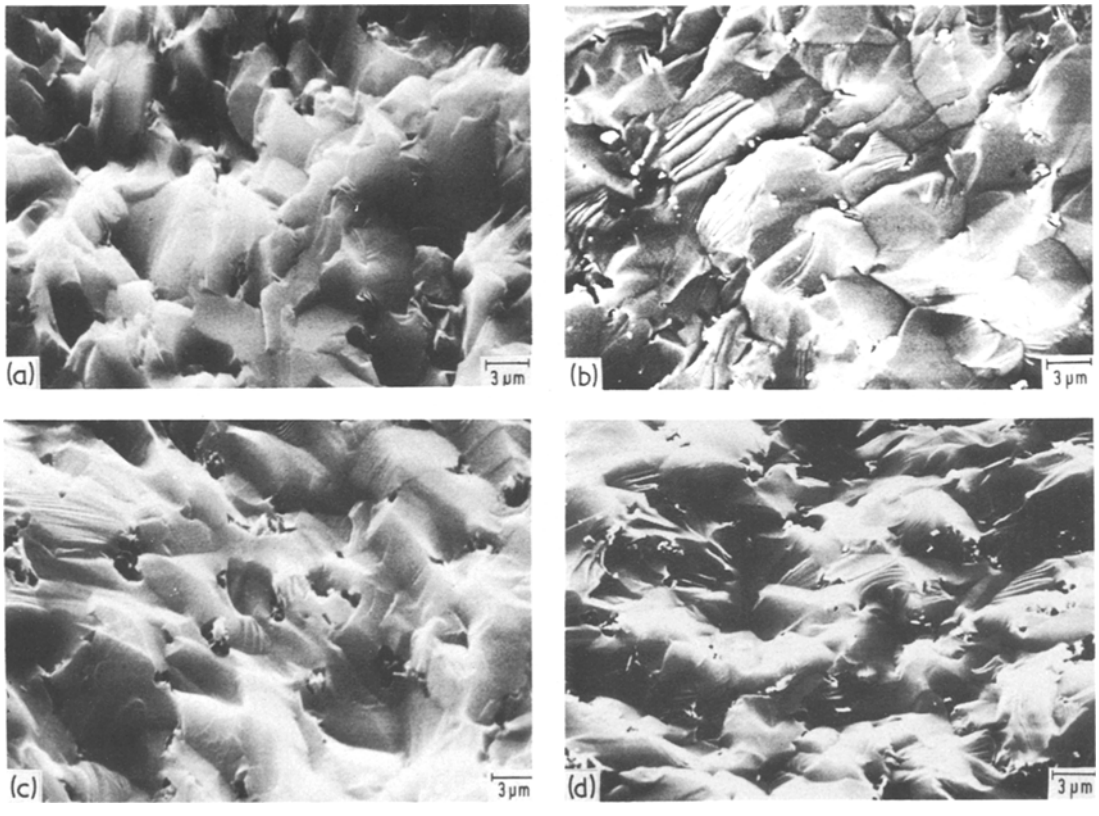

Figure 3 SEMs of fracture surfaces: (a) SSiC I; (b) SSiC II; (c) SSiC III; (d) SSiC IV.

O-containing inclusions together with Ca and in some cases with Al, have been analysed in material II. In Fig. 5 the spectrum from a point analysis of such an inclusion, here Ca and O, is reproduced.

Besides these characteristics many foreign phases and inclusions enriched by impurities and sintering additives and with very different chemical compositions have been analysed. In a few cases it was even impossible to detect Si and/or C. Metallic Al was present and some small Al-silicate inclusions were found in material I. The impurity elements: B, N, O, Na, K, Ca, Cr, Fe, Ni, Cu were detected by AES in this material.

In material II heterogeneous regions (up to 200 μm diameter) with B-, O-, N-, Na-, Al-, S-, K- and Ca-enrichments were analysed, which covered about 10% of the investigated fracture surfaces. The element distribution of B, K, Na, O and the spectra of two point analyses (A and B) from sample II are presented in Fig. 6. The content of K, Ca and Na was enormous in some inclusions. Owing to the moderate O-content, silicates from the systems Si–O–K, Si–O–Ca, Si–O–Na, may be present.

4.2. Wavelength dispersive analysis of X-rays

Specimens of lots I, II and III were investigated. It was necessary to work with a very low acceleration voltage (13 kV) and a relative high current of the beam (100 nA) in order to achieve a signal level sufficient for the analyses. For the same reason the electron beam could not be focused to its minimal value and therefore the lateral resolution was only around 3 μm. The specimens were embedded in an electrical conducting resin, ground and polished.

4.2.1. Al-doped SSiC I

From several point analyses, an Al content of 0.55% was measured (0.4% by chemical analysis, Table II).

Flat-shaped inclusions were found by imaging the specimen by absorbed electrons and taking up the element distributions of O and Al, which

exhibit strong enrichments. The concentration profiles across this inclusion demonstrated very intense enrichments of Al, O and also C. These inclusions exist possibly as Al-silicates in addition to free carbon.

4.2.2. B-doped SSiC II

Absorbed electron imaging of this polished specimen exhibits a number of striking bright inclusions up to 2.5 μm diameter as shown in Fig. 10 together with the concentration profile. It is easy to see that the three inclusions coincide with the three peaks of the boron profile. Because of the lack of a suitable standard, these B-enriched phases could not be determined quantitatively. The inclusions contain only very small amounts of C and an Si concentration similar to the matrix.

In Fig. 8 the concentration profiles of Si, Al and Mg along the line in the Al-distribution photograph are presented. The Si-concentration of the matrix is determined to be about 70%. One of the two areas with very low Si concentration coincides with Al- and Mg-enrichments. These areas contain extremely small O- and C-concentrations. The Al content of the matrix was approximately 0.05%; in this Al-rich phase a maximum value of 4.3% was found. Other microstructural details are presented in Fig. 9. Ca-, O- and C-concentration profiles are shown, which reveal the existence of CaO inclusions and of free C.

Further regions were found whose absorbed electron images showed bright inclusions up to 15 μm in diameter. The distribution maps of the elements Al, O and C demonstrate enrichments of these elements, similar to the flat-shaped

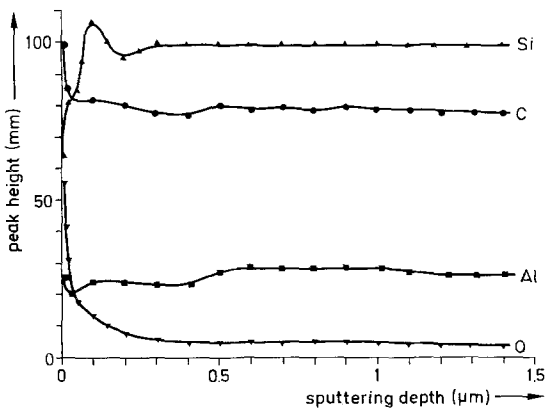

Figure 4 AES depth analysis of a selected Al-rich area in the fracture surface of SSiC I.

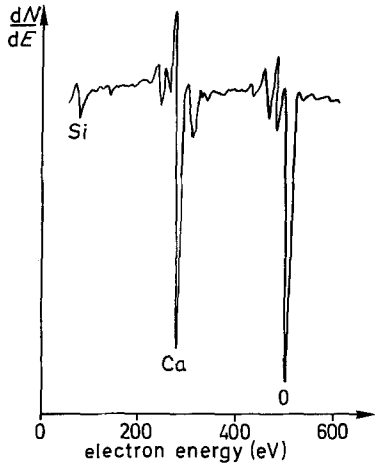

Figure 5 AES point analysis on an O- and Ca-rich inclusion in the fracture surface of SSiC II.

inclusions found in material I. Both the absorbed electron image and the distribution can be seen in Fig. 10. Element concentration profiles were drawn up across the bright inclusion, from Fig. 10. Very large amounts of impurities, nominal N, O, Mg, Al, Ca and also C, were detected. The Al-, O- and Ca-enrichment, particularly, in this inclusion were rather high (Al content around 30%); simultaneously, the Si content can be virtually neglected. The question of the presence of ternary, binary or elementary phases in this region remains open so far.

4.2.3. B-doped SSiC III

The B distribution of this material appears to be inhomogeneous. B was analysed in addition to Si and C in single grains, as shown in Fig. 11. Simultaneously with the very large B content, the Si concentration decreased in this grain although this is not shown in this figure.

4.3. Microautoradiography

This method allows a semi-quantitative statement of the concentration and spatial distribution of α-particle emitting nuclides. Applied to the present work the method gives information about the B distribution, especially in B-doped sintered SiC. B has a very high efficiency for the following nuclear reaction with thermal neutrons:

$$^{10}_{5}B + {}^{1}_{0}n \rightarrow {}^{7}_{3}Li + {}^{4}_{2}He.$$

The emitted α-particles enter a few microns of a detector foil which is faced upon a polished specimen during irradiation. The ionizing α-radiation

injures the foil. By etching the foil in NaOH the impacts can be made visible. The detection limit of this technique is in the range of 10^{-6}. Our irradiation experiments were performed in the FR 2 research reactor of the Kernforschungszentrum Karlsruhe. The thermal neutron flow was 2.3×10^{11} n cm^{-2} sec^{-1} and variable irradiation times were used. So far results have been received from materials II and IV. In Fig. 12 the relative uniform B-distribution of material II is compared with the rather inhomogeneous distribution of material IV.

It is not possible to detect B-enrichments on the grain boundaries or in single grains. The reason may be found in the formation depth of the α-particles, which is in the same range as the average grain size. Thus, the emitting particles will probably scatter a few microns when leaving the specimen surface before they hit the foil. The impacts are often fused together to form craters by the etching process and cannot be identified separately. Nevertheless, the degree of uniformity of the B-distribution in different samples can be clearly distinguished.

4.4. Scanning transmission electron microscopy

The first aim in using transmission electron microscopy in this study was to investigate the grain boundaries. The lateral resolutions of the WDX- and EDX-techniques are not sufficient to analyse the virtually pure grain boundaries of sintered SiC. By AES these analyses are possible under extremely clean conditions*. Other reasons for the use of TEM/STEM are the investigation of very small inclusions (e.g. at the triple points), of dislocations, stacking faults and the structure analysis of the phases present. Initial results on material I are shown in the following figure. The micrographs were made with a 100 kV STEM. Fig. 13 was taken from a region near the border of a hole. An inclusion in a triple point with a diameter of less than 0.1 μm is shown in the bright-field and the dark-field image. Isolated inclusions but no continuous layers have been found at the grain boundaries in this material so far. It should be noted that the given real resolution of our equipment was about 5 nm with the foil used.

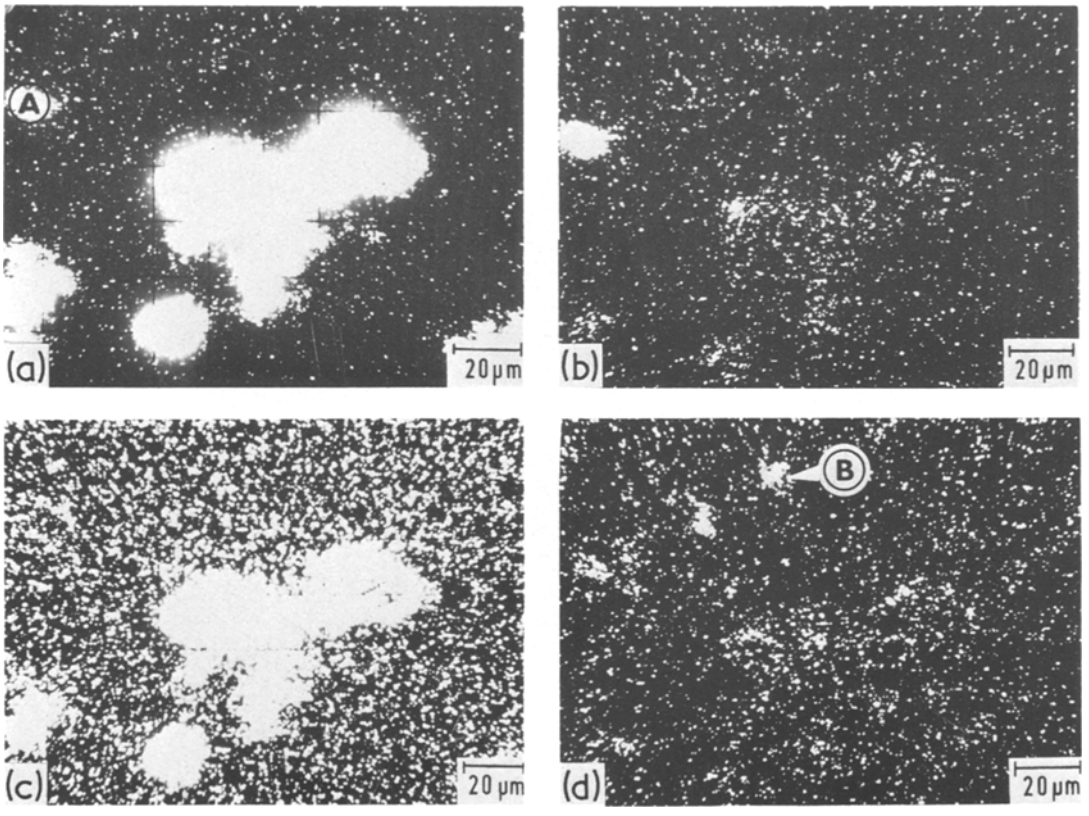

Figure 6 Fracture surface of SSiC II analysed by AES. Distribution maps of (a) B, (b) K, (c) Na, (d) O and (e) AES spectra at points A and B.

*This will be published soon in a second part of this paper.

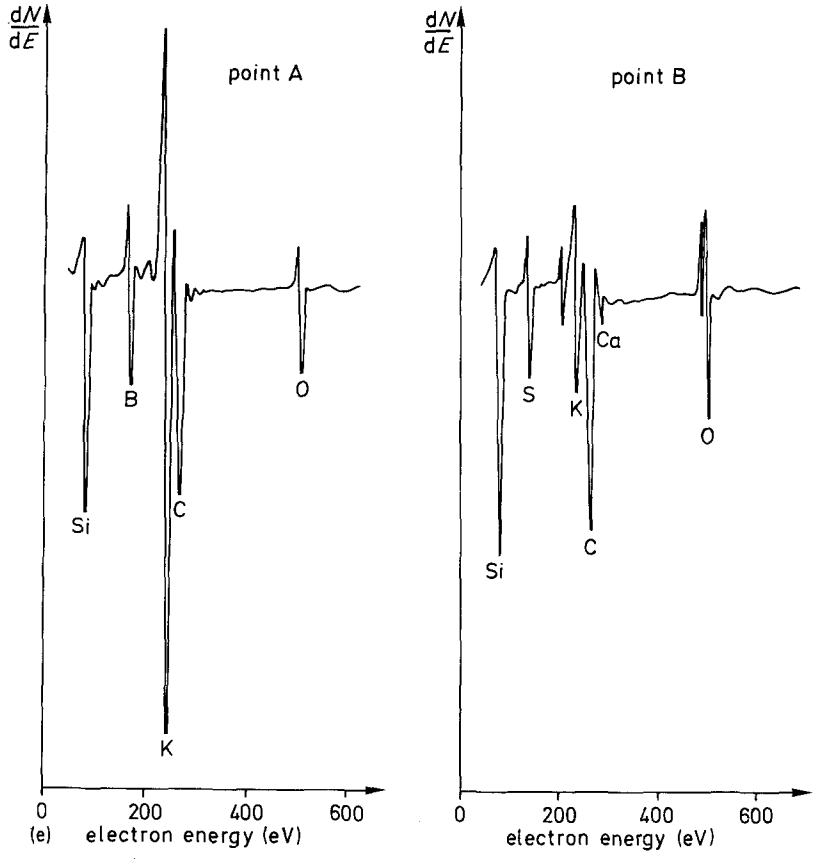

Figure 6 continued.

5. Discussion

The results of this study indicate that all the SSiC-materials investigated contain enrichments of impurities and sintering additives with very high concentrations at certain spots in the microstructures.

The results of the AES and WDX investigations are generally in a good agreement with each other.

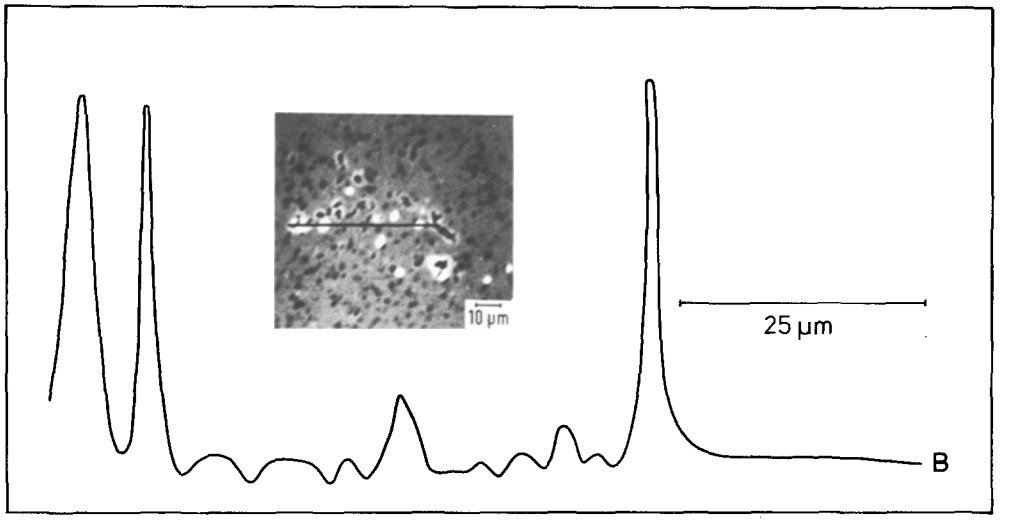

Figure 7 Absorbed electron image and B-line profile in SSiC II.

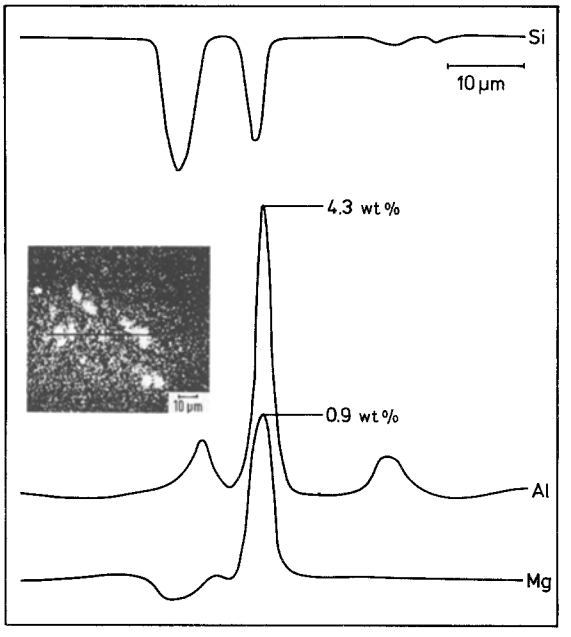

Figure 8 Al distribution map and line profiles of Si, Al and Mg in SSiC II.

This is remarkable considering the very different information depths and the fact that the specimens were prepared in different ways for both methods. The AES measurements, in combination with ion sputtering, allowed investigation and analysis of fractured areas, while polished specimens were used for WDX measurements. The constant Al content in the matrix, without any significant variation at the grain boundaries, as measured by WDX can be interpreted as a solid solution of Al in the bulk material. The B segregations and inclusions with a very high B content cannot be detected in the α-microautoradiograms of these materials because of insufficient resolution in this technique. Nevertheless, the inhomogeneity of the B distribution in SSiC IV was demonstrated by α-microautoradiography. Information from AES and WDX studies about this material will be reported in the future.

A large number of different-sized inclusions consisting of impurities, and also in combination with sintering additives, were found by AES and WDX. These inclusions are thought to have a detrimental influence on the mechanical properties. The very large inhomogeneous areas detected on the fracture surfaces by AES could, in particular, be responsible for the initiation of intergranular fracture processes. Special attention should be drawn to those areas where extremely high concentrations exist, e.g. approximately 30% Al in material II.

The inhomogeneity of the B distribution and the large Al-rich areas lead to the question whether the amounts of the sintering additives are chosen and admixed properly with respect to an optimal microstructure. Generally, this inhomogeneous distribution of the additives may inhibit their optimal function during sintering. It cannot be postulated, however, that the microstructural inhomogeneities detected in the sintered samples are the same as in the green compacts before sintering, but nevertheless, the presence of considerable inhomogeneities in the green samples must be assumed.

6. Conclusion

Detailed and fairly comprehensive knowledge about the microstructure of sintered silicon carbide materials has been achieved by the combined use of different microanalytical methods. This aim can only be reached by the mutual

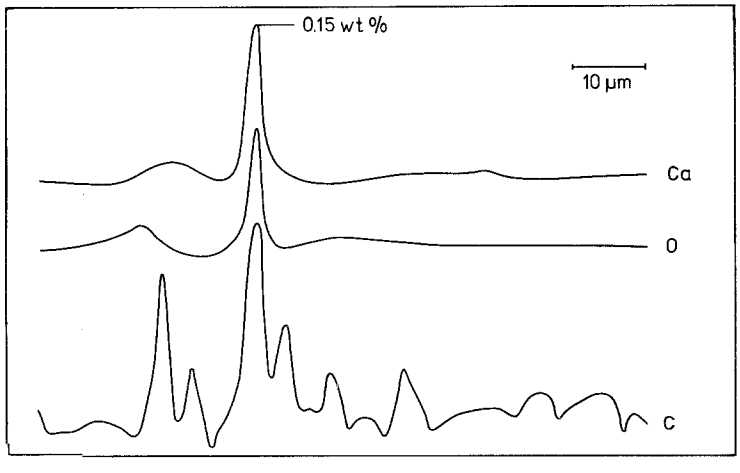

Figure 9 Concentration profiles of Ca Ca, O and C along the line shown in Fig. 11.

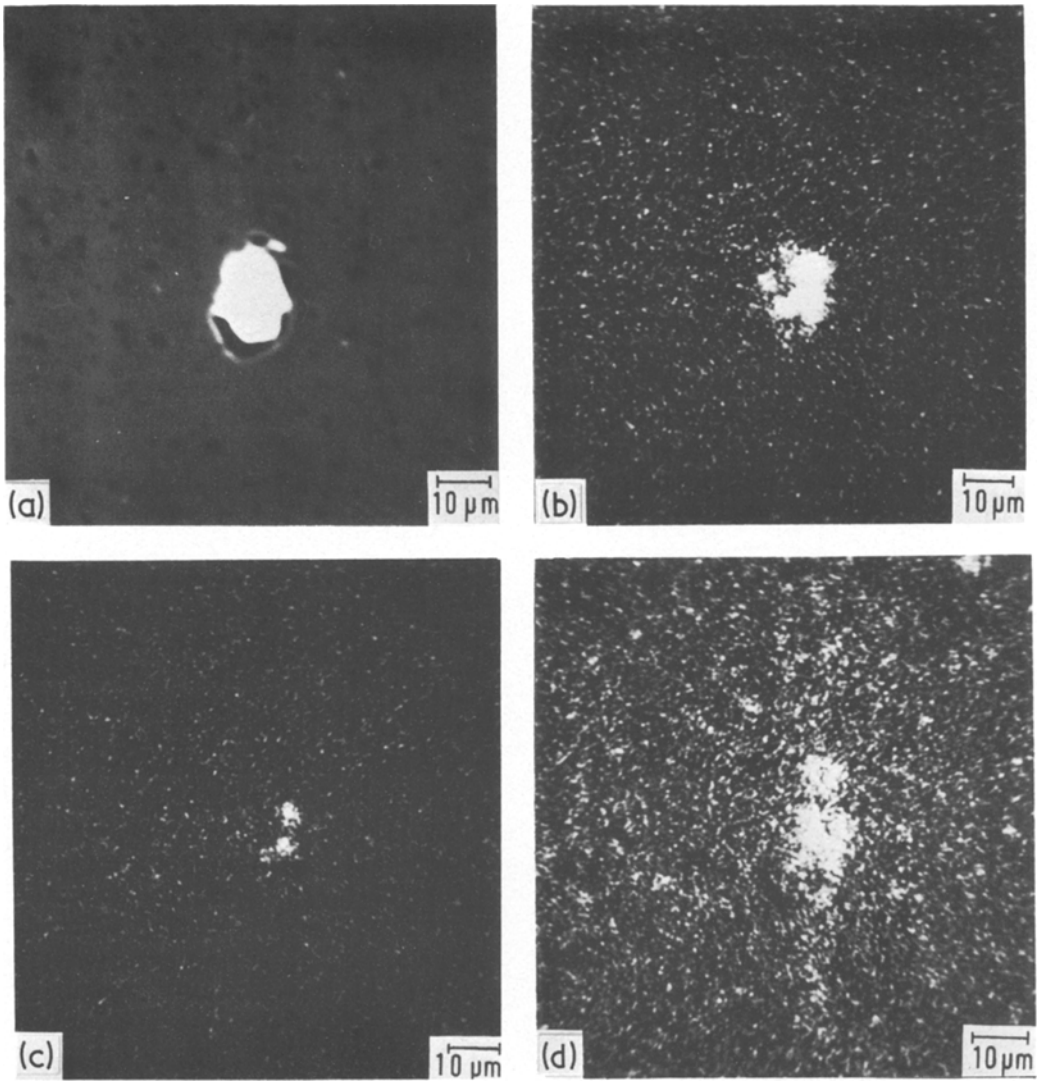

Figure 10 (a) Absorbed electron image of an inclusion, and distribution maps of (b) Al, (c) O and (d) C in SSiC II.

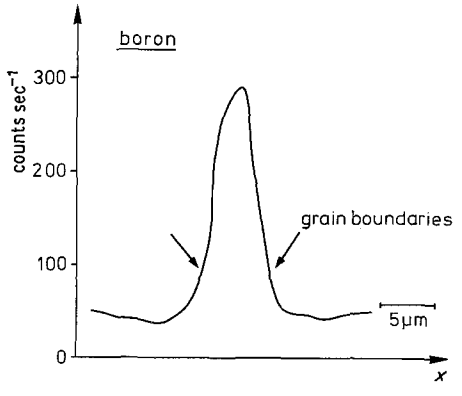

Figure 11 WDX profile of B across an SSiC III surface with maximal concentration in the interior of a grain.

completion of the various microanalytical techniques and by the additional results of the fundamental ceramography and chemical analysis. The microstructural inhomogeneity is demontrated by a large number of inclusions and precipitations with high concentrations of additives and impurities. The results of this investigation demonstrates that the manufacturing process of sintered silicon carbide has not been fully optimized so far. The production process should be improved, e.g. by the application of pure starting powders and the control of the powder processing variables including sintering additives. In the future, a high-quality sintered SiC will certainly exhibit an improved homogeneity of

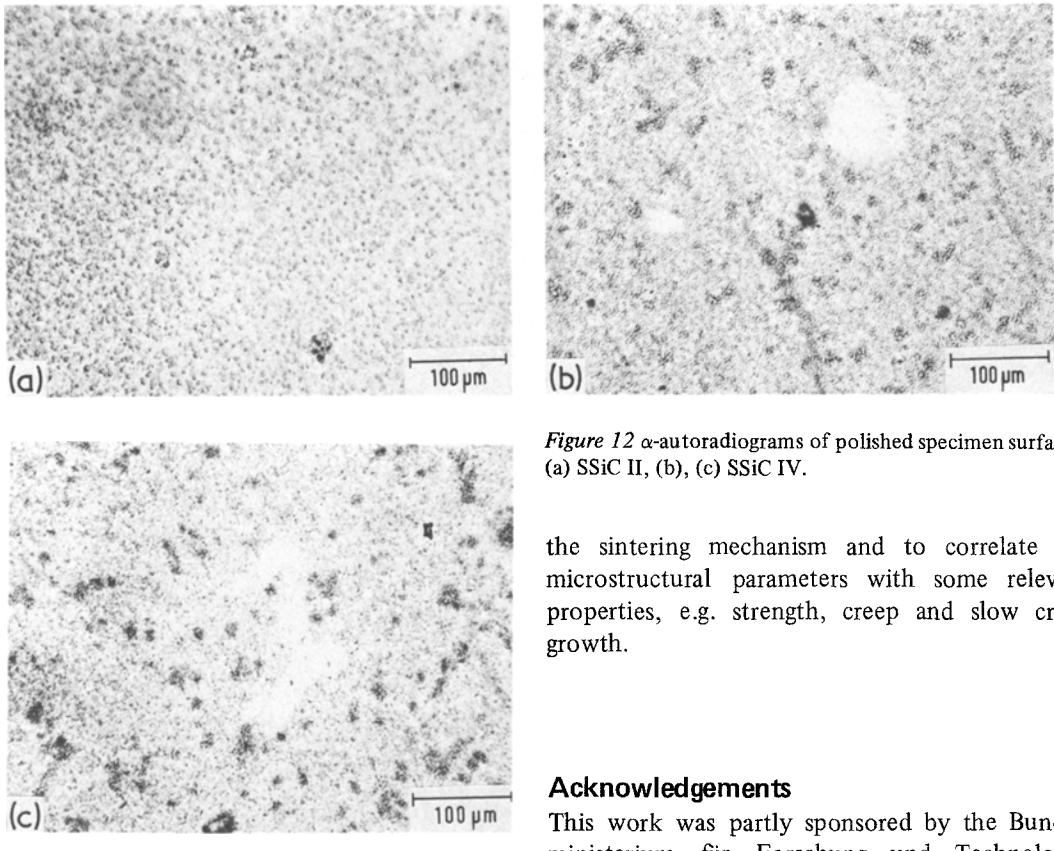

Figure 12 α-autoradiograms of polished specimen surfaces: (a) SSiC II, (b), (c) SSiC IV.

the microstructure with respect to the distribution of the intentional additives and the impurities. Continuing this combined study a body of knowledge is to be elaborated in order to understand the sintering mechanism and to correlate the microstructural parameters with some relevant properties, e.g. strength, creep and slow crack growth.

Acknowledgements

This work was partly sponsored by the Bundesministerium für Forschung und Technologie, Bonn. The authors are grateful to Dr Ch. Braun, Dr H. Kleykamp and their co-workers for the chemical analysis and the analytical work of AES and WDX.

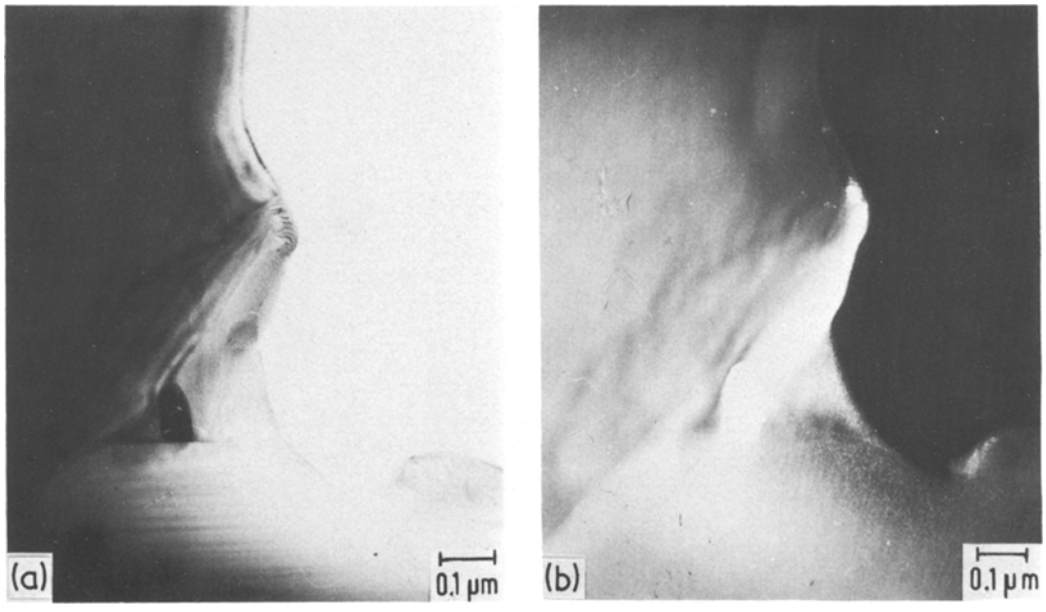

Figure 13 STEM micrographs of a triple-point region of SSiC I: (a) bright-field; (b) dark-field.

References

1. S. PROCHAZKA, "Ceramics for high performance applications", edited by J. J. Burke *et al.* (Brook Hill, Chestnut Hill, 1974) p. 239.
2. H. HAUSNER, "Energy and Ceramics", edited by P. Vincenzini (Elsevier, Amsterdam, New York, Oxford, 1980) p. 582.
3. K. A. SCHWETZ and A. LIPP, *Sci. Ceram.* **10** (1980) 149.
4. S. PROCHAZKA, "Mass Transport Phenomena in Ceramics", edited by A. R. Cooper and A. H. Heuer, Material Science Research, Vol. 9 (Plenum Press, New York 1975) p. 421.
5. F. F. LANGE and T. K. GUPTA, *J. Amer. Ceram. Soc.* **59** (1976) 537.
6. W. BÖCKER and H. HAUSNER, *Powder Met. Int.* **10** (1978) 87.
7. G. GRATHWOHL, TH. REETZ and F. THÜMMLER, *Sci. Ceram.* **11** (1981).
8. R. HAMMINGER, Diploma thesis, University of Karlsruhe (1980).
9. Y. TAJIMA and W. D. KINGERY, in "Basic research in crystalline and noncrystalline ceramic systems". Department of Materials Science and Engineering Ceramics Division, Massachusetts Institute of Technology, Cambridge, Mass. Annual Report, 1 August 1980 to 31 October 1981, p. 31.

Received 25 March
and accepted 8 May 1982